Chemical Engineering Journal 158 (2010) 599–607

Contents lists available at ScienceDirect

Chemical Engineering Journal

journal homepage: www.elsevier.com/locate/cej

# Arsenite and arsenate adsorption on coprecipitated bimetal oxide magnetic nanomaterials: $MnFe_2O_4$ and $CoFe_2O_4$

Shengxiao Zhang, Hongyun Niu, Yaqi Cai*, Xiaoli Zhao, Yali Shi

*State Key Laboratory of Environmental Chemistry and Ecotoxicology, Research Center for Eco-Environmental Science, Chinese Academy of Sciences, Beijing 100085, China*

ARTICLE INFO

*Article history:*
Received 21 August 2009
Received in revised form 5 February 2010
Accepted 6 February 2010

*Keywords:*
Magnetic nanomaterials
Arsenic
Adsorption
Desorption
Surface hydroxyl

ABSTRACT

Bimetal oxide magnetic nanomaterials ($MnFe_2O_4$ and $CoFe_2O_4$) were synthesized and characterized with transmission electron microscope (TEM), X-ray powder diffraction (XRD), vibrating sample magnetometer (VSM), and X-ray photoelectron spectroscopy (XPS). The adsorption of arsenic on these nanomaterials was studied as a function of pH, initial arsenic concentration, contact time and coexisting anions. The Langmuir and Freundlich isotherm models were applied to fit the adsorption data, and the maximum adsorption capacities of arsenite ($As^{III}$) and arsenate ($As^{V}$) on $MnFe_2O_4$ were 94 and 90 mg $g^{-1}$, and on $CoFe_2O_4$ were 100 and 74 mg $g^{-1}$, respectively. $MnFe_2O_4$ and $CoFe_2O_4$ showed higher $As^{III}$ and $As^{V}$ adsorption capacities than the referenced $Fe_3O_4$ (50 and 44 mg $g^{-1}$, respectively) prepared by the same procedure. Quantificational calculation from XPS narrow scan results of O(1s) spectra of adsorbents indicated that the higher adsorption capacities of $As^{III}$ and $As^{V}$ on $MnFe_2O_4$ and $CoFe_2O_4$ than on $Fe_3O_4$ might be caused by the increase of the surface hydroxyl (M–OH) species. Phosphate and silicate were powerful competitors with arsenic for adsorptive sites on the adsorbent. Desorption study showed that over 80% of $As^{III}$ and 90% of $As^{V}$ could be desorbed from $MnFe_2O_4$ with 0.1 M NaOH solution.



## 1. Introduction

Arsenic contaminations in natural water and wastewater have been considered as serious problems. Arsenic pollution has been reported recently in USA, China, Chile, Bangladesh, Taiwan, Mexico, Argentina, Poland, Canada, Hungary, New Zealand, Japan and India. Millions of people are at the risk of chronic arsenic poisoning in Bangladesh and West Bengal in India [1]. Long-term drinking water containing arsenic causes various cancer as well as skin lesions, hyperkeratosis, and melanosis. The World Health Organization (WHO) has amended the maximum permissible limited arsenic concentration in drinking water from 50 to 10 μg $L^{-1}$, and the U.S. Environmental Protection Agency (EPA) has adopted an arsenic maximum contaminant level of 10 μg $L^{-1}$ [2]. Therefore, effective treatment techniques for arsenic removal must be taken to meet the standard.

Arsenic exists usually as inorganic forms in natural environment. Arsenate ($As^{V}$) is dominant in aerobic environments, and arsenite ($As^{III}$) exists in moderately reducing anaerobic environments. The p$K_a$ values indicate that arsenite exists predominately as $H_3AsO_3^0$ (p$K_{a1}$ = 9.2, p$K_{a2}$ = 12.1, and p$K_{a3}$ = 12.7) and arsenate as $H_2AsO_4^-$ and $HAsO_4^{2-}$ (p$K_{a1}$ = 2.3, p$K_{a2}$ = 6.9, and p$K_{a3}$ = 11.5) in natural aqueous environments [3]. Arsenite is usually considered more toxic, soluble and mobile than arsenate [4]. Unfortunately arsenite has been detected at levels from 100 to 2000 μg $L^{-1}$ in the groundwater of many countries.

Many different methods, including precipitation, ion-exchange, adsorption and membrane filtration, have been studied for arsenic removal [5–8]. Among them adsorption is regarded as a promising technology for its easy operation, low cost and little by-products. Various natural and synthetic materials have been used to adsorb arsenic from aqueous solution [9–11]. In recent years some researchers have prepared bimetal oxide adsorbents for arsenic adsorption. Zhang et al. [12] found that a Fe–Ce bimetal adsorbent with appropriate ratio showed a significantly higher $As^{V}$ adsorption capacity than the referenced Ce and Fe oxides prepared by the same procedure. Deschamps et al. [13] used a natural Fe–Mn-mineral material in a packed-bed column to remove arsenic from As-spiked tap water and a mining effluent. Zhang et al. [4,14] developed a Fe–Mn binary oxide adsorbent for effective $As^{III}$ removal, and they reported that the manganese dioxide oxidized $As^{III}$ to $As^{V}$, then $As^{V}$ was adsorbed by the original adsorption sites on iron oxide and the newly formed adsorption sites during $As^{III}$ oxidation. Masue et al. [3] studied arsenic adsorption/desorption behavior on Fe–Al hydroxide. They found that when Fe:Al molar ratio was 4:1 the bimetal hydroxide adsorbent gained approximately equal

* Corresponding author at: Chinese Academy of Sciences, Research Center for Eco-Environmental Sciences, P.O. Box 2871, Beijing 100085, China.
Tel.: +86 010 62849239; fax: +86 010 62849182.
*E-mail address:* caiyaqi@rcees.ac.cn (Y. Cai).

1385-8947/$ – see front matter © 2010 Elsevier B.V. All rights reserved.
doi:10.1016/j.cej.2010.02.013

$As^V$ adsorption capacity to iron hydroxide, but the $As^{III}$ adsorption capacity on iron hydroxide was higher than that on the Fe–Al hydroxide.

Nanomaterials, possessing high surface area and excellent adsorption ability, have received extensive attentions in the field of pollutant adsorption and environmental remediation. They also have been widely studied for arsenic adsorption [15–17], but the difficulty to separate solids from solution limits their practical application. Magnetic nanoparticles of $Fe_3O_4$ can be separated from solution by using an external magnetic field, and the adsorption ability of this material has been studied in recent years [18,19]. In this study, we investigated the adsorption behavior of $As^{III}$ and $As^V$ on bimetal oxide magnetic nanomaterials: $MnFe_2O_4$ and $CoFe_2O_4$. A single metal oxide, $Fe_3O_4$ prepared following the same procedure, was used in comparison study. Bimetal oxide magnetic nanomaterials combined the virtue of bimetal oxide adsorbents, nanomaterials and magnetic materials. Arsenic adsorption on bimetal oxide magnetic nanomaterials was seldom reported previously. The objectives of this study were to (i) prepare and characterize bimetal oxide magnetic nanomaterials, (ii) examine the stability of these magnetic bimetal materials under different pH solutions, (iii) investigate the adsorption and desorption behaviors of arsenic on these materials, and (iv) discuss the possible adsorption mechanism.

## 2. Experimental

### 2.1. Materials and chemicals

All reagents used in the experiment were analytical reagent grade and used without further purification. The $As^{III}$ and $As^V$ stock solutions were prepared by dissolving $NaAsO_2$ and $Na_2HAsO_4{\bullet}7H_2O$ obtained from Beijing Chemicals Corporation (Beijing, China) in deionized water. Potassium borohydride ($KBH_4$), ferric chloride ($FeCl_3{\bullet}6H_2O$) and ferrous chloride ($FeCl_2{\bullet}4H_2O$) were purchased from Tianjin Jinke Chemical Reagent Corporation (Tianjin, China). Cobalt (II) nitrate ($Co(NO_3)_2{\bullet}6H_2O$) and manganese (II) nitrate ($Mn(NO_3)_2$) were supplied by Sinopharm Chemical Reagent Co., Ltd. (Shanghai, China). Ultrapure water was prepared by using Milli-Q water purification system (Millipore, Bedford, MA, USA).

### 2.2. Adsorbents preparation

$MnFe_2O_4$ magnetic nanoparticles were prepared by the chemical coprecipitation method. $Mn(NO_3)_2$ (1.8 g) and $FeCl_3{\bullet}6H_2O$ (5.2 g) were dissolved into 25 mL deoxygenated water followed by adding 0.85 mL of concentrated hydrochloric acid. The resulting solution was dropped into 250 mL of 1.5 M NaOH solution under vigorous stirring and $N_2$ protection at 353 K. The obtained nanoparticles were separated from solution by a magnet and rinsed with 50 mL deionized water for two times. Finally the products were dispersed into 110 mL deionized water to get 20 mg $mL^{-1}$ suspension of $MnFe_2O_4$. The similar procedure was applied to prepare $CoFe_2O_4$ and $Fe_3O_4$ magnetic nanoparticles with $Co(NO_3)_2{\bullet}6H_2O$, $FeCl_3{\bullet}6H_2O$ and $FeCl_2{\bullet}4H_2O$.

### 2.3. Batch adsorption tests

Arsenic adsorption experiments were performed in 50 mL polypropylene bottles containing 20 mL aqueous solution. The concentration of adsorbent was 0.2 g $L^{-1}$. Ionic strength was adjusted to 0.01 M with 1 M $NaNO_3$ solution, and solution pH was adjusted with $HNO_3$ and NaOH to designated values. Then the suspensions were stirred at room temperature for 24 h. Effect of solution pH on the adsorption of arsenic was investigated with a fixed $As^{III}$ or $As^V$ concentration (10 mg $L^{-1}$) at pH 3–10. Adsorption kinetic study was carried out following the above adsorption procedure at the intervals of time: 0.167, 0.5, 1, 2, 4, 8, 12, 22, 24 h. Adsorption isotherms were obtained by varying initial arsenic concentration (0.5–50 mg $L^{-1}$). $Na_2SiO_3$, $Na_3(PO_4)_2$, $Na_2CO_3$ and $Na_2SO_4$ were added into the solution to test the effects of coexisting anions on arsenic adsorption.

After adsorption, the bottle was placed on a magnet for a few seconds to separate the adsorbents from aqueous solution. When the solution became limpid, a portion of supernatant was diluted to 10 mL with hydrochloric acid solution (10%, v/v). The arsenic concentration in diluted solution was determined with an AF-610A HG-AFS instrument (Beijing Ruili Analytical Instrument Co., Ltd., China). Hydrochloric acid solution (10%, v/v) was used as carrying fluid. Duplicate adsorption experiments were performed, and averaged results were reported. To investigate the leaching of metal ion, $Fe_3O_4$, $MnFe_2O_4$, and $CoFe_2O_4$ were immerged into aqueous solution with pH ranging from 3 to 11 and stirred for 24 h, then the concentration of metal ions in the supernatant was determined with ICP-AES (Leeman Labs, Hudson, NH) after the adsorbents were separated.

Desorption tests were carried out using sodium hydroxide solution in the range of 0.01–1.5 M. The adsorbents after adsorption of $As^{III}$ or $As^V$ were mixed with 2 mL × 3 desorption solution. The mixture was shaken for 1 h, and then the adsorbents were separated with an external magnetic field. The desorption efficiency was calculated from the amount of arsenic in supernatant.

### 2.4. *Characterization of adsorbents*

The morphology and particle size of the adsorbents were studied by using a transmission electron microscope (TEM) of H-7500 (Hitachi, Japan) operating at 80 kV accelerated voltage. Magnetic property of the adsorbents was analyzed using a vibrating sample magnetometer (VSM, LDJ9600). An X-ray powder diffractometer (Rigaku III/B max) was used to analyze the crystalline structures of adsorbents. The point of zero charge (PZC) of the materials was determined with zetasizer 2000 apparatus (Malvern, United Kingdom). The specific surface areas of adsorbents were determined by the BET method with $N_2$ gas (ASAP2000V3.01A; Micromeritics, Norcross, GA, USA).

To detect the binding energies and atomic ratio of the adsorbents surface, some selected samples were freeze-dried for further analysis using X-ray photoelectron spectroscopy (XPS) collected on an ESCA-Lab-220i-XL spectrometer with monochromatic Al Kα radiation (1486.6 eV). C1s peaks were used as an inner standard calibration peak at 284.7 eV. Thermogravimetry and differential thermal analysis (TG–DTA) for freeze-dried samples were carried out on a Mettler Toledo Star TGA/SDTA 851 apparatus, and the temperature ranged from room temperature to 1273 K with rising rate of 10 K $min^{-1}$. The sample chamber was purged with dry nitrogen.

## 3. Results and discussion

### 3.1. *Characterization of $MnFe_2O_4$, $CoFe_2O_4$, and $Fe_3O_4$*

The specific surface areas of $MnFe_2O_4$, $CoFe_2O_4$, and $Fe_3O_4$ were 138, 101, and 102 $m^2$ $g^{-1}$, respectively. Fig. 1(a)–(c) shows TEM images of $MnFe_2O_4$, $CoFe_2O_4$ and $Fe_3O_4$. These adsorbents were all quasi-spherical in shapes, and their diameters were about 30–50, 10–30 and 10–20 nm, respectively. The PZC of these nanomaterials was determined by their zeta potential in solution at varying pH. As shown in Fig. 2(a), the PZC of $CoFe_2O_4$ was almost identical to that of $Fe_3O_4$ ($pH_{PZC}$ 7.0), while $MnFe_2O_4$ possessed a relatively higher

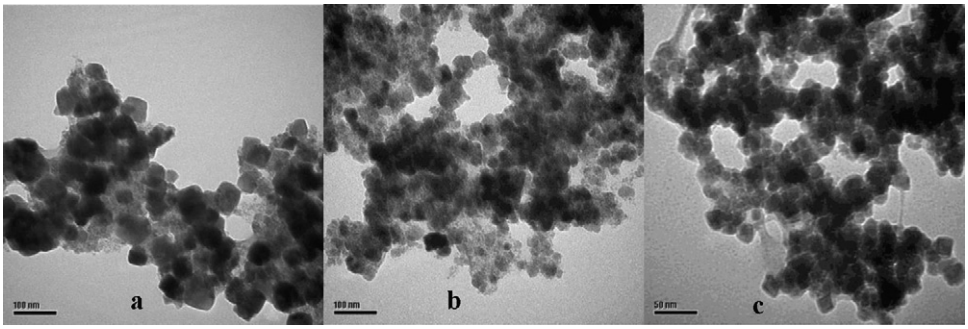


**Fig. 1.** TEM images of (a) $MnFe_2O_4$, (b) $CoFe_2O_4$, and (c) $Fe_3O_4$ MNPs.

PZC ($pH_{PZC}$ 7.5) than $Fe_3O_4$ and $CoFe_2O_4$. XRD patterns of $MnFe_2O_4$, $CoFe_2O_4$ and $Fe_3O_4$ MNPs are shown in Fig. 2(b). Bragg reflections for $MnFe_2O_4$ and $CoFe_2O_4$ could be indexed to spinel ferrites, and $Fe_3O_4$ to cubic crystalline bulk magnetite. As determined by XPS in Fig. 2(c), the surface molar ratio of Fe/Mn or Fe/Co for $MnFe_2O_4$, $CoFe_2O_4$ were all 2:1, which were in accordance with the metal ion ratio in solution as these materials were totally dissolved in HCl solution. Similar results were observed by energy dispersive spectrometer (EDS) analysis (data not shown).

The hysteresis loops of adsorbents were investigated to check for their paramagnetic behavior. Fig. 2(d) shows that there was small hysteresis in the hysteresis loops of these adsorbents, and the remanence of $MnFe_2O_4$, $CoFe_2O_4$ and $Fe_3O_4$ were 3.49, 8.46 and 0.70 emu $g^{-1}$, and the coercivity were 48, 242 and 3 Oe, respectively. The low remanence and coercivity indicated the paramagnetism of these magnetic nanoparticles. The maximal saturation magnetization of $MnFe_2O_4$, $CoFe_2O_4$ and $Fe_3O_4$ were 32.02, 46.99 and 55.41 emu $g^{-1}$, respectively. Since saturation magnetization of 16.3 emu $g^{-1}$ was enough for magnetic separation from solution with a magnet [20], the paramagnetic properties and large saturation magnetization made these adsorbents readily separated from solution by applying an external magnetic field. When the external magnetic field was taken away these nanoparticles could be redispersed rapidly.

The concentrations of dissolved metal ion under different pH are shown in Fig. 3. The metal ion concentrations were all below 5 mg $L^{-1}$ under tested pH range. When the solution pH was over 6, the leached Fe, Mn, Co concentrations were below 1 mg $L^{-1}$. The relatively low metal leakage would not cause metal pollution in environment, indicating the good stability of these adsorbents.

### 3.2. *Effect of pH*

The adsorption trends of $As^{III}$ and $As^{V}$ on $MnFe_2O_4$, $CoFe_2O_4$ and $Fe_3O_4$ under different initial pH are shown in Fig. 4(a) and (b). It could be concluded that pH had no obvious effect on $As^{III}$ adsorption. Similar phenomena had been reported when iron oxide minerals were used to adsorb arsenic [21]. In our study $As^{III}$ existed predominately as $H_3AsO_3^0$ under the designed pH range, therefore the effects of solution pH on $As^{III}$ adsorption was hardly observed. In the subsequent $As^{III}$ adsorption experiments, the solution pH was set at 7 unless especially pointed out.

As shown in Fig. 4(b), $As^{V}$ adsorption was evidently dependent on pH, and the uptake was high under acidic conditions. In the pH

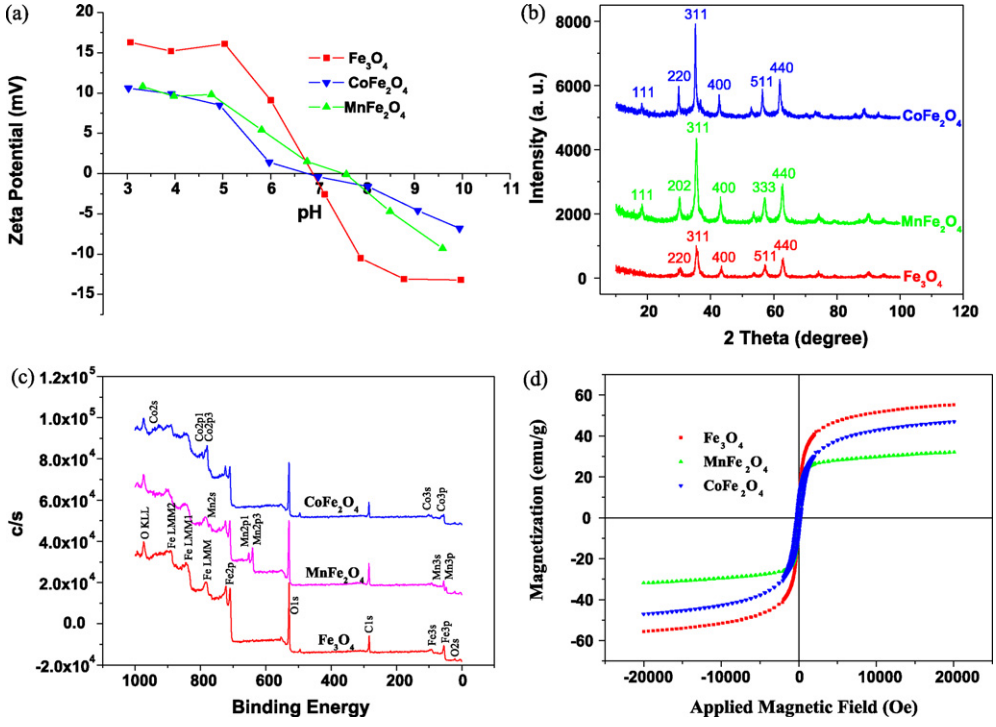


**Fig. 2.** (a) Zeta potential as a function of pH; (b) X-ray diffraction pattern; (c) wide XPS scan; and (d) VSM curves of $Fe_3O_4$, $MnFe_2O_4$, and $CoFe_2O_4$ MNPs.

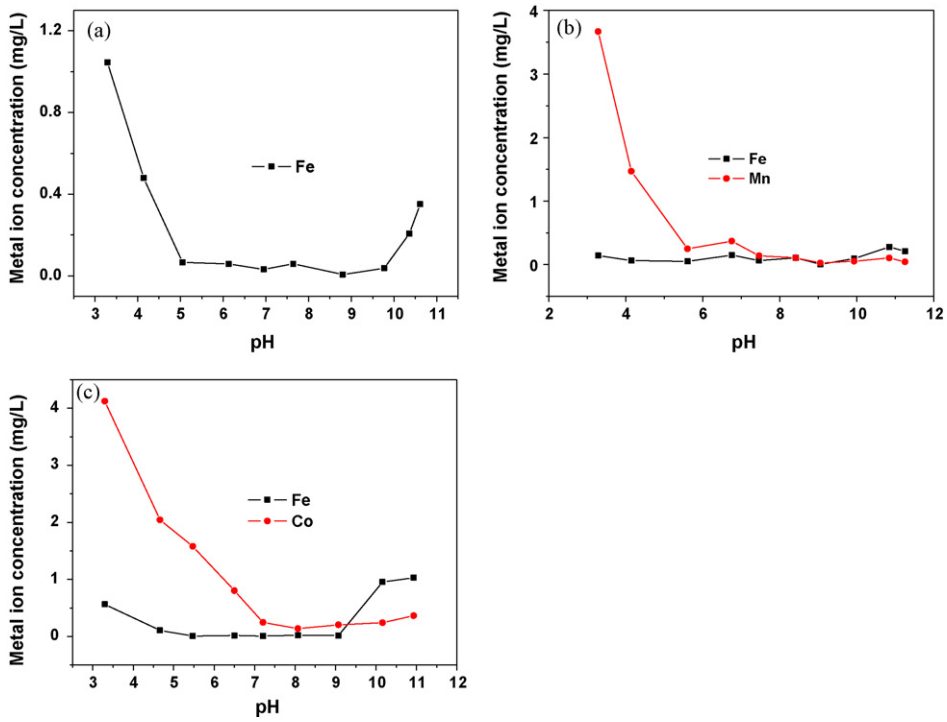


**Fig. 3.** Metal ion concentrations leached out from (a) $Fe_3O_4$, (b) $MnFe_2O_4$, and (c) $CoFe_2O_4$ MNPs under different pH solutions.

range of 3–10, $H_2AsO_4^-$ and $HAsO_4^{2-}$ were dominant $As^V$ species. At pH below PZC of adsorbents, the surface hydroxyl groups were protonated to form $OH_2^+$ [22], which facilitated ligand exchange with arsenate anion [3]. With the increase of solution pH, the gradual deprotonation of surface hydroxyl groups made the adsorbents negatively charged, which imposed repulsion with the anionic $As^V$ and was unfavorable for $As^V$ adsorption.

### 3.3. *Adsorption isotherms*

Adsorption isotherms of $As^{III}$ were conducted at pH 7.0, and $As^V$ at pH 3.0. Langmuir and Freundlich isotherm models were used to analyze the equilibrium date.

$$\frac{C_e}{q_e} = \frac{1}{\theta b} + \frac{C_e}{\theta} \quad (1)$$

$$\log\ q_e = \log K_F + \frac{1}{n}\ \log C_e \quad (2)$$

where $q_e$ (mg g$^{-1}$) and $C_e$ (mg L$^{-1}$) were the equilibrium adsorption capacity and the equilibrium adsorbate concentration; $\theta$ was the maximum adsorption capacity and $b$ was the equilibrium adsorption constant. The maximum adsorption capacity ($\theta$) could be calculated from the slope of the linear plot of $C_e/q_e$ versus $C_e$. $K_F$ (mL$^{1/n}$ μg$^{1-1/n}$) and $n$ were the Freundlich constants. The value of $n$ and $K_F$ could be obtained from slope of linear plot of log $q_e$ versus log $C_e$.

The equilibrium data for $As^{III}$ and $As^V$ adsorption are shown in Fig. 5. As a result, $MnFe_2O_4$ and $CoFe_2O_4$ had higher adsorption capacity for $As^{III}$ and $As^V$ than $Fe_3O_4$. The equilibrium data were analyzed by Langmuir and Freundlich isotherm models. The related parameters are shown in Table 1. Regression coefficients ($R^2$) for different conditions were larger than 0.97, indicating that both Langmuir and Freundlich models were suitable for describing the adsorption behavior of arsenic on bimetal oxide magnetic nanomaterials. The application of the Langmuir isotherm model is based on monolayer coverage of adsorbent surfaces by the adsorbate. The Freundlich isotherm model is an empirical equation based on the multilayer adsorption of an adsorbate onto heterogeneous surfaces. It is valid for adsorption data over a restricted range of concentrations. The maximum adsorption capacities ($\theta$) of $As^{III}$ on $MnFe_2O_4$ and $CoFe_2O_4$ calculated from Langmuir adsorption isotherm were 94 and 100 mg g$^{-1}$, and for $As^V$ were 90 and 74 mg g$^{-1}$, respectively, which were about two times as high as those obtained on the referenced $Fe_3O_4$ (50 and 44 mg g$^{-1}$ for $As^{III}$ and $As^V$, respectively) prepared following the same procedure. Compared with other Fe and metal/Fe oxides (Table 2), $MnFe_2O_4$ and $CoFe_2O_4$ magnetic nanomaterials were effective for both $As^{III}$ and $As^V$ adsorption. Therefore, we had attained the aim of developing ideal adsorbents

**Table 1**
Langmuir and Freundlich isotherm parameters for adsorption of $As^{III}$ and $As^V$ on $MnFe_2O_4$, $CoFe_2O_4$ and $Fe_3O_4$.

| As species | Adsorbent | Langmuir model | | | Freundlich model | | |
|---|---|---|---|---|---|---|---|
| | | $\theta$ (mg g$^{-1}$) | $b$ (L mg$^{-1}$) | $R^2$ | $K_F$ (mg$^{1-1/n}$ L$^{1/n}$ g$^{-1}$) | $n$ | $R^2$ |
| $As^{III}$ | $MnFe_2O_4$ | 93.8 | 0.450 | 0.984 | 29.6 | 2.83 | 0.996 |
| | $CoFe_2O_4$ | 100.3 | 0.599 | 0.985 | 36.9 | 3.13 | 0.992 |
| | $Fe_3O_4$ | 49.8 | 0.248 | 0.976 | 15.2 | 3.35 | 0.998 |
| $As^V$ | $MnFe_2O_4$ | 90.4 | 2.59 | 0.999 | 59.7 | 7.48 | 0.990 |
| | $CoFe_2O_4$ | 73.8 | 1.44 | 0.998 | 49.4 | 9.08 | 0.998 |
| | $Fe_3O_4$ | 44.1 | 0.458 | 0.987 | 19.2 | 4.34 | 0.978 |

As (V) at pH 3.0, As (III) at pH 7.0, adsorbent, 0.2 g L$^{-1}$, 25 °C.

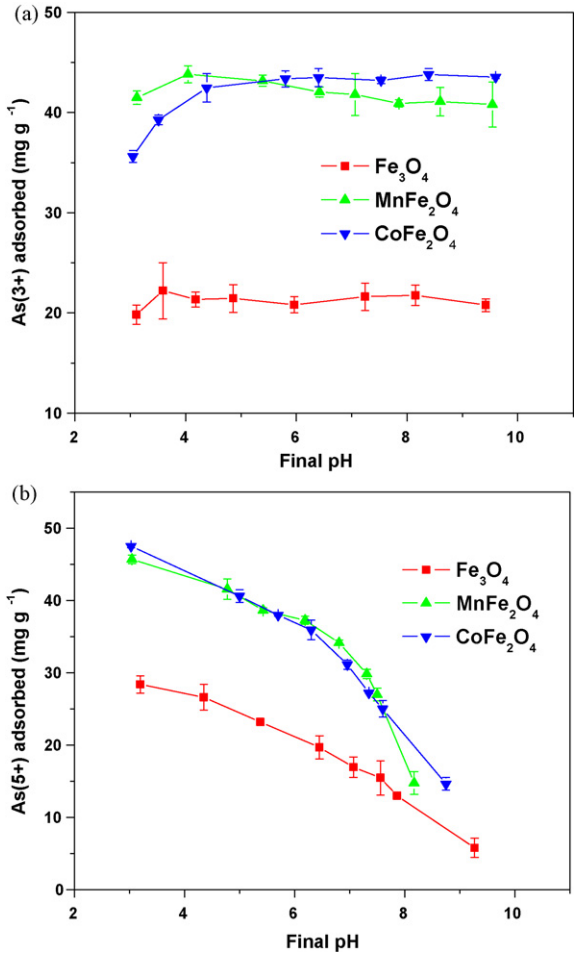


**Fig. 4.** Effect of pH on adsorption of (a) $As^{III}$ and (b) $As^{V}$ on $MnFe_2O_4$, $CoFe_2O_4$, and $Fe_3O_4$ MNPs. Reaction condition: 10 mg $L^{-1}$ $As^{III}$ or $As^{V}$ adsorbed on 0.2 g $L^{-1}$ adsorbents in 0.01 M $NaNO_3$ solution.

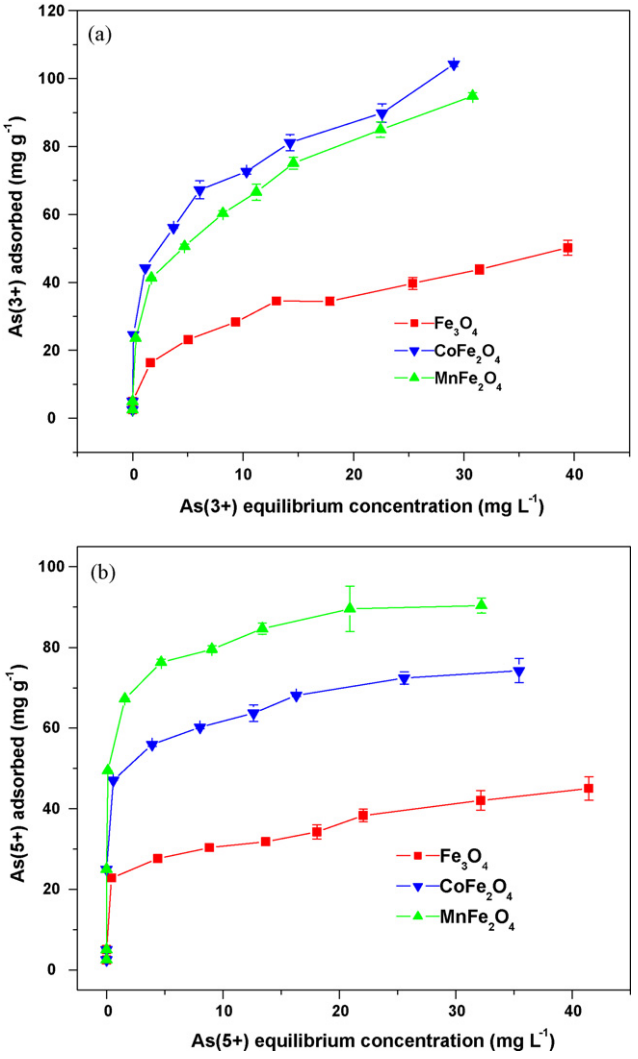


**Fig. 5.** Adsorption isotherms of arsenic on $MnFe_2O_4$, $CoFe_2O_4$, and $Fe_3O_4$ MNPs (0.2 g $L^{-1}$) in 0.01 M $NaNO_3$: (a) $As^{III}$ at pH 3 and (b) $As^{V}$ at pH 7.

possessing both high arsenic adsorption capacity and paramagnetism for magnetic separation.

$CoFe_2O_4$ and $Fe_3O_4$ exhibited similar surface areas, and $MnFe_2O_4$ had a surface area about 30% greater than that of $CoFe_2O_4$ and $Fe_3O_4$. While the adsorption capacity of arsenic on $MnFe_2O_4$ and $CoFe_2O_4$ were about two times higher than that obtained on $Fe_3O_4$ adsorbents, indicating that surface area was not the main factor to determine arsenic adsorption capacity on these nanomaterials. Surface property, especially surface hydroxyl group (M–OH), usually was considered to affect arsenic adsorption. The element information on the surface of $MnFe_2O_4$, $CoFe_2O_4$, and $Fe_3O_4$ was studied by XPS. The O(1s) spectra of each material are shown in Fig. 6(a)–(c). The O(1s) spectrum was composed of overlapped peaks of oxide oxygen ($O^{2-}$), hydroxyl (–OH), and sorbed water ($H_2O$). All of the spectra were fitted using a 50:50 Gaussian:Lorentzian peak shape [12,23], and satisfactory fitting results were obtained as shown in Fig. 6(a)–(c) and Table 3. Generally, $O^{2-}$ was the most abundant oxygen species in the O(1s) spectra of $MnFe_2O_4$, $CoFe_2O_4$, and $Fe_3O_4$ (45.19, 47.99 and 63.69%, respectively). Hydroxyl group (M–OH) was the second important oxygen species on the surface of these adsorbents and occupied 40.42 and 38.09% of the total oxygen species in $MnFe_2O_4$ and $CoFe_2O_4$, respectively, which was much higher than that of $Fe_3O_4$ (25.37%). This result indicated that the replacement of $Fe^{2+}$ with $Mn^{2+}$ and $Co^{2+}$ resulted in a significant increase of the M–OH species in magnetic nanomaterials. Arsenic adsorption was reported to carry out

**Table 2**
Maximum arsenic adsorption capacities of some adsorbents.

| Adsorbent | Maximum $As^{III}$ adsorption capacity (mg $g^{-1}$) | Maximum $As^{V}$ adsorption capacity (mg $g^{-1}$) | Ref. no. |
|---|---|---|---|
| $Fe_3O_4$ | 49.8 | 44.1 | Present study |
| $MnFe_2O_4$ | 93.8 | 90.4 | Present study |
| $CoFe_2O_4$ | 100.3 | 73.8 | Present study |
| Fe–Mn composite | 132.61 | 69.68 | [4] |
| Fe–Mn-mineral | 11.99 | 6.74 | [13] |
| Fe–Ce composite | – | 149.84 | [12] |
| Fe–Ti composite | 85 | 14.3 | [16] |
| Fe–Al hydroxides | 42.72 | 78.62 | [3] |
| goethite | – | 5 | [26] |

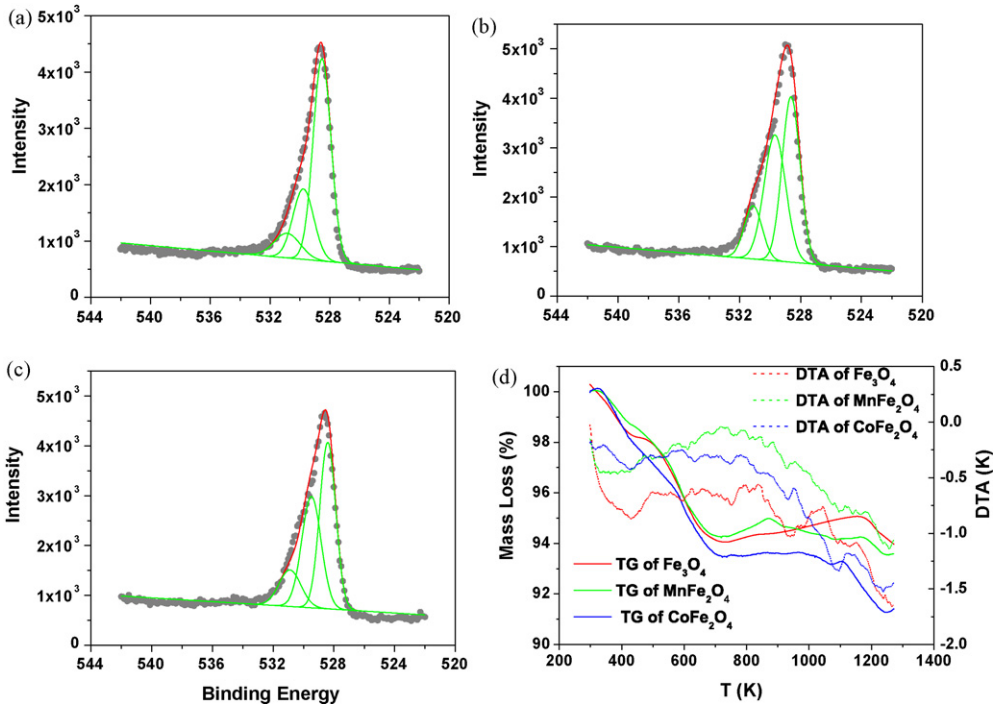


**Fig. 6.** O(1s) spectra of (a) $Fe_3O_4$, (b) $MnFe_2O_4$, and (c) $CoFe_2O_4$; (d) TG–DTA curves. The red curves are the best fit to the spectral data. The green curves represent photopeak contributions from $O^{2-}$, $OH^-$ and $H_2O$. The peak at the lowest binding energy is oxide ($O^{2-}$), the peak with intermediate binding energy is $OH^-$, and the highest energy peak is that of $H_2O$. (For interpretation of the references to colour in this figure legend, the reader is referred to the web version of the article.)

through the replacement of the hydroxyl group of metal oxide with arsenate and arsenite to form monodentate, bidentate mononuclear and bidentate binuclear complex [12,22]. So the higher arsenic adsorption capacity of bimetal oxide magnetic nanomaterials than that of $Fe_3O_4$ might be owed to the increased M–OH contents.

To further investigate the surface hydroxyl group of sorbents, TG/DTA analysis was applied, and the results are shown in Fig. 6(d). The first part of mass loss, which was obviously observed between room temperature and 423 K in TG curve of $Fe_3O_4$, was the weight of physically adsorbed water. The next mass losses corresponding to chemisorption water (surface hydroxyl group) for $MnFe_2O_4$, $CoFe_2O_4$, and $Fe_3O_4$ were 4.521, 4.737, and 4.093%. The content of surface hydroxyl groups of $MnFe_2O_4$ and $CoFe_2O_4$ were higher than $Fe_3O_4$, and the results were in accordance with XPS analysis.

### 3.4. Adsorption kinetics study

In this study, the kinetics of arsenic adsorption was conducted to investigate the adsorption rate. Fig. 7(a) and (c) shows the changes of $As^{III}$ and $As^{V}$ concentration in solution with time. The adsorption of arsenic was rapid in the first 2 h, and then slowed down, and 12 h of contact time was enough to reach equilibrium. From Fig. 7 we concluded that the adsorption of $As^{V}$ required less time to reach equilibrium than that of $As^{III}$. The initial fast adsorption of $As^{III}$ and $As^{V}$ might be due to the nanoscaled particle size of adsorbents, since fine particles was favorable for the diffusion of arsenic molecules from bulk solution onto the active sites of the adsorbents [4]. The following slow adsorption rate in Fig. 7 suggested that the adsorption was controlled dominantly by intraparticle diffusion.

**Table 3**
O(1s) peak parameters for different materials.

| Adsorbent | Peak[a] | Binding energy | Percent[b] |
|---|---|---|---|
| $Fe_3O_4$ | $O^{2-}$ | 528.5 | 63.69 |
| | $OH^-$ | 529.8 | 25.37 |
| | $H_2O$ | 530.8 | 10.94 |
| $MnFe_2O_4$ | $O^{2-}$ | 528.6 | 45.19 |
| | $OH^-$ | 529.7 | 40.42 |
| | $H_2O$ | 531.1 | 14.39 |
| $CoFe_2O_4$ | $O^{2-}$ | 528.4 | 47.99 |
| | $OH^-$ | 529.5 | 38.09 |
| | $H_2O$ | 530.9 | 13.92 |

[a] Surface species: $O^{2-}$, oxygen bonded to metal; $OH^-$, hydroxyl bonded to metal; $H_2O$, sorbed water.
[b] The percentage represents the contribution of each peak to the total number of counts under the O(1s) peak.

To quantify the changes of arsenic adsorption with time on different adsorbents, we used pseudo-second-order equation [24] to describe the adsorption of arsenic on magnetic nanomaterials:

$$\frac{t}{q_t} = \frac{1}{kq_e^2} + \frac{1}{q_e}t \quad (3)$$

where $k$ is the rate constant of adsorption (g mg$^{-1}$ min$^{-1}$), $q_t$ is the amount of arsenic adsorbed by adsorbent at any time (mg g$^{-1}$), $q_e$ is equilibrium adsorption capacity (mg g$^{-1}$), and the initial sorption rate, $h$ (mg g$^{-1}$ min$^{-1}$) can be defined as:

$$h = kq_e^2 \quad (t \to 0) \quad (4)$$

Both $k$ and $h$ can be determined experimentally from the slope and intercept of plot of $t/q_t$ versus $t$. The kinetics of arsenic adsorption onto magnetic nanomaterials fit well with the pseudo-second-order kinetic model ($R^2 > 0.99$). The constant $k$ and initial sorption rate $h$ obtained from the slope and intercept of plots are presented in Table 4. The $h$ and $k$ values of $As^{V}$ were higher than those of $As^{III}$, indicating the faster adsorption rate of $As^{V}$ than that of $As^{III}$. The rate constants of $As^{III}$ and $As^{V}$ adsorption on $Fe_3O_4$ were higher than that on $MnFe_2O_4$ and $CoFe_2O_4$, which demonstrated that $Fe_3O_4$ nanoparticles required less time to reach equilibrium.

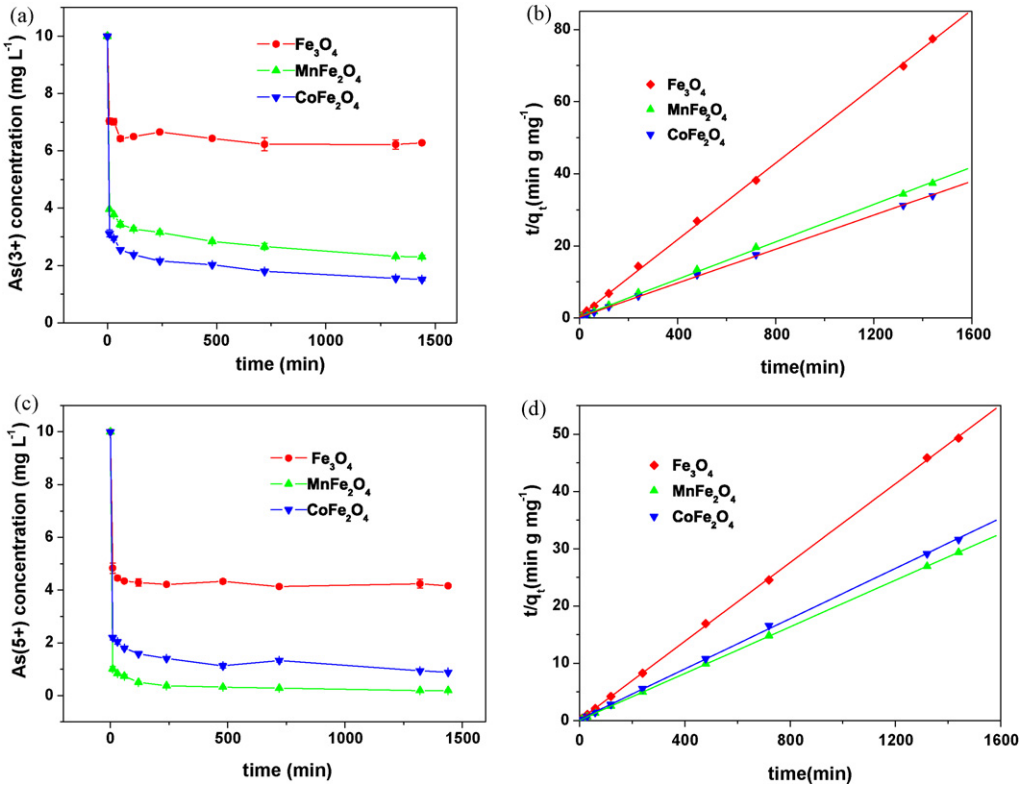


**Fig. 7.** Adsorption kinetics of arsenic on $MnFe_2O_4$, $CoFe_2O_4$, and $Fe_3O_4$ MNPs (0.2 g $L^{-1}$) in 0.01 M $NaNO_3$: (a) $As^{III}$ at pH 3; (b) pseudo-second-order kinetic plot for $As^{III}$; (c) $As^{V}$ at pH 7, and (d) pseudo-second-order kinetic plot for $As^{V}$.

### 3.5. *Effect of competing anions*

Competition of natural water constituents with arsenic for adsorptive sites mainly arose from anions, especially oxyanions. So four oxyanions ($SO_4^{2-}$, $CO_3^{2-}$, $SiO_3^{2-}$, $PO_4^{3-}$) were selected to investigate the effect of coexisting anions on arsenic adsorption on $MnFe_2O_4$, and the concentrations of four oxyanions were set at 0.1, 1.0, 10.0 mM. When effect of $SO_4^{2-}$ and $PO_4^{3-}$ was tested, the pH was fixed at 7.0 for $As^{III}$ and 3.0 for $As^{V}$. In order to avoid the converting of $CO_3^{2-}$ to $CO_2$ and the formation of amorphous $SiO_2$ solids in acid conditions, the solution pH was not adjusted when competitive adsorption between arsenic and $CO_3^{2-}$ or $SiO_3^{2-}$ was investigated. The corresponding solution pH with 0, 0.1, 1.0, 10.0 mM $CO_3^{2-}$ or $SiO_3^{2-}$ was 7.0, 8.08, 10.30, 11.02 or 7.0, 8.15, 10.75, 11.90, respectively. The effect of competing anions on arsenic adsorption is shown in Fig. 8(a) and (b). $SO_4^{2-}$ had little effect on $As^{III}$ and $As^{V}$ adsorption. The addition of $CO_3^{2-}$ decreased arsenic adsorption moderately. The decrease of adsorption ability might result from two factors: firstly, the strong basic condition was unfavorable for $As^{V}$ adsorption due to the addition of $Na_2CO_3$. Secondly, arseno–carbonate complexes, including $As(CO_3)_2^-$, $As(CO_3)(OH)_2^-$ and $AsCO_3^+$, might form in the presence of high concentration of $CO_3^{2-}$ in solution [25], which prevented arsenic from forming

**Table 4**
Pseudo-second-order rate constants for $As^{V}$ and $As^{III}$ adsorption onto adsorbents.

| As species | Adsorbent | $k$ (g $mg^{-1}$ $min^{-1}$) | $h$ (mg $g^{-1}$ $min^{-1}$) | $R^2$ |
|---|---|---|---|---|
| $As^{III}$ | $MnFe_2O_4$ | $1.70 \times 10^{-3}$ | 2.53 | 0.9996 |
| | $CoFe_2O_4$ | $2.06 \times 10^{-3}$ | 3.71 | 0.9998 |
| | $Fe_3O_4$ | $5.77 \times 10^{-3}$ | 2.05 | 0.9997 |
| $As^{V}$ | $MnFe_2O_4$ | $6.38 \times 10^{-3}$ | 15.37 | 0.9999 |
| | $CoFe_2O_4$ | $2.61 \times 10^{-3}$ | 5.40 | 0.9998 |
| | $Fe_3O_4$ | $1.88 \times 10^{-2}$ | 15.91 | 0.9999 |

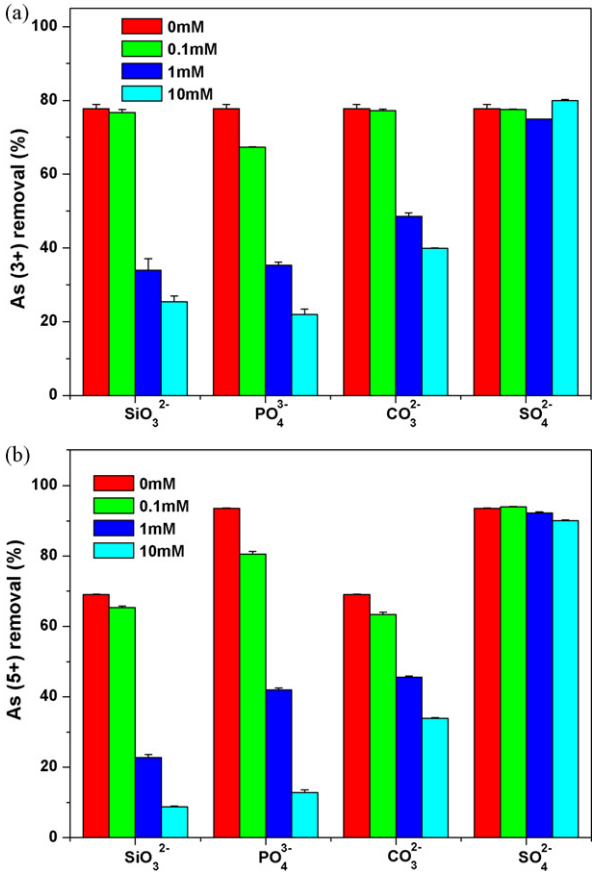


**Fig. 8.** Effect of competing anions on (a) $As^{III}$ and (b) $As^{V}$ adsorption on $MnFe_2O_4$ MNPs.

inner-sphere complexes on the surface of adsorbents. As shown in Fig. 8, the adsorption of $As^{III}$ and $As^{V}$ was greatly affected by the $PO_4^{3-}$ and $SiO_3^{2-}$ anion. When the concentration of the two anions was 0.1 mM, the removal efficiency was decreased by 10–20%. With the increase of $PO_4^{3-}$ and $SiO_3^{2-}$ concentration, the adsorption of arsenic decreased greatly. It is reported that arsenate, phosphate and silicate are all tetrahedral anions, and they all can form inner-sphere complexes with the hydroxyl groups at the surface of adsorbents [17,25]. The decrease of arsenic removal might result from the competition between $PO_4^{3-}$ or $SiO_3^{2-}$ and arsenic for adsorption sites. Another possible reason for the negative effect of $SiO_3^{2-}$ on arsenic adsorption was the high solution pH, which was unfavorable for $As^{V}$ adsorption.

### 3.6. Desorption study

To test the feasibility of bimetal oxide magnetic nanomaterials to be regenerated after adsorption of arsenic, desorption study was carried out with $MnFe_2O_4$ adsorbent. At high pH, the surface hydroxyl groups got deprotonated and negatively charged, resulting in efficiently desorption of negatively charged arsenic species [22]. Hence sodium hydroxide solution was used to desorb the adsorbed arsenic from adsorbent. As a result, with 0.1 M NaOH solution, 80% of $As^{III}$ and 90% of $As^{V}$ adsorbed on adsorbents were released. If the concentration of NaOH was increased to 1 M, 87% of $As^{III}$ and 99% of $As^{V}$ could be desorbed. Due to the paramagnetism of magnetic nanomaterials, they could be readily separated from solution with magnetic field after adsorption or desorption of arsenic, which would facilitate the reuse of magnetic nanomaterials.

### 3.7. Adsorption mechanism

In Fig. 9(a) and (b), As(3d) spectra of $MnFe_2O_4$ and $CoFe_2O_4$ after adsorption of $As^{III}$ and $As^{V}$ showed only one peak, the binding energy of 44.6 and 46.0 eV should be attributed to $As^{III}$–O and $As^{V}$–O, respectively. It could be suggested that there was little $As^{III}$ oxidized into $As^{V}$ in the adsorption procedure. Fig. 10(a)–(c) shows the zeta potentials of $Fe_3O_4$, $MnFe_2O_4$ and $CoFe_2O_4$ in the presence or absence of $As^{III}$ and $As^{V}$. As a result, the PZC of adsorbents decreased obviously after arsenic adsorption expect for $As^{III}$ adsorbed $Fe_3O_4$. It was reported that the formation of outer-sphere surface complexes could not shift the PZC of metal oxide because there was no specific chemical reactions between the adsorbate

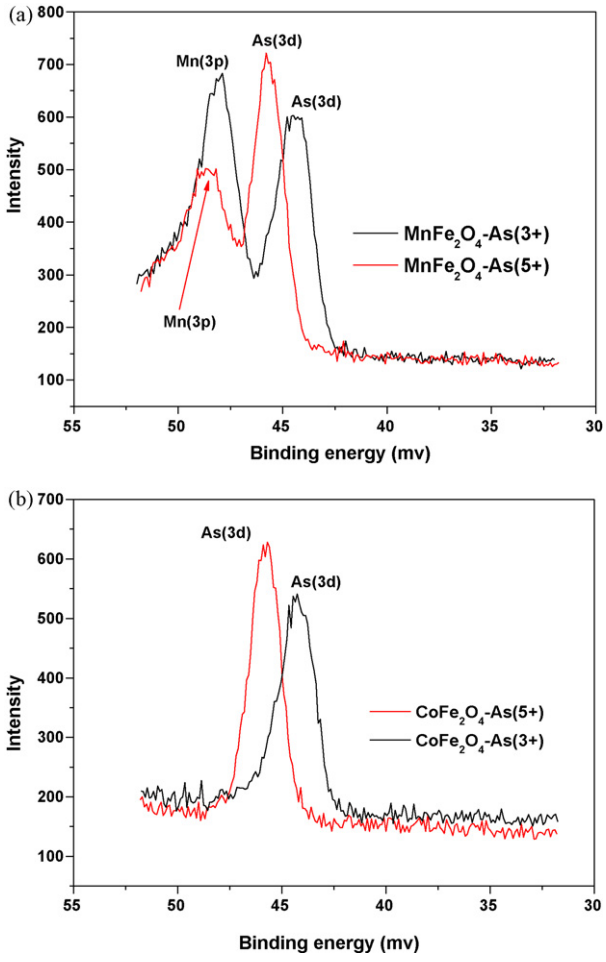


**Fig. 9.** As (3d) spectra of (a) $MnFe_2O_4$ and (b) $CoFe_2O_4$ after adsorption of $As^{III}$ and $As^{V}$.

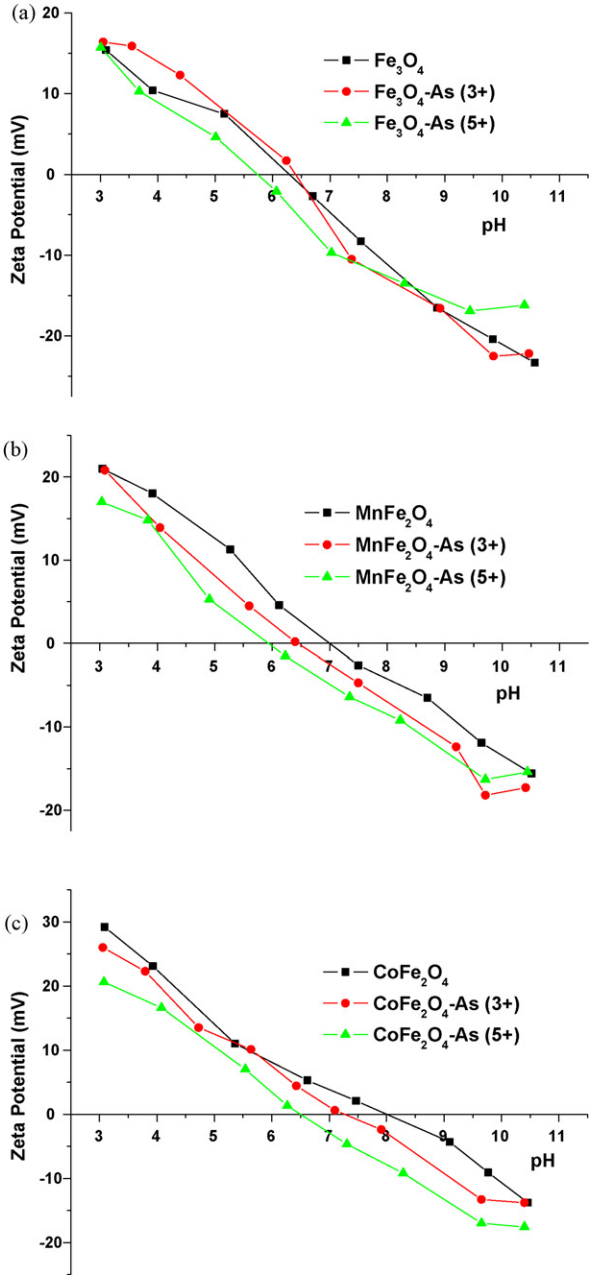


**Fig. 10.** Zeta potential of (a) $Fe_3O_4$, (b) $MnFe_2O_4$, and (c) $CoFe_2O_4$ as a function of pH in 50 mM NaCl solution in the absence or presence of 1 mg $L^{-1}$ $As^{III}$ and $As^{V}$.

and the adsorbent that could change the surface charge. The shift of PZC to a lower pH range was evidence of the formation of anionic negatively charged surface complexes [2]. Therefore the decrease of PZC implied that the adsorption of arsenic would be based on the negatively charged inner-sphere complexes between $As^{V}$ or $As^{III}$ and adsorbents.

## 4. Conclusions

Bimetal oxide magnetic nanomaterials had been synthesized and applied to adsorb arsenic from aqueous solution. The maximum adsorption capacities of $As^{III}$ and $As^{V}$ on $MnFe_2O_4$ and $CoFe_2O_4$ were higher than on the referenced $Fe_3O_4$. XPS and TG analysis of adsorbents indicated that the higher adsorption capacity of arsenic on $MnFe_2O_4$ and $CoFe_2O_4$ than on $Fe_3O_4$ might be caused by the increase of the surface hydroxyl groups. Phosphate and silicate were powerful competitors with arsenic for adsorptive sites on the adsorbent. Adsorbed arsenic could be desorbed easily from adsorbents with NaOH solution, and adsorbents could be separated from solution using a magnet due to their paramagnetism. The shift of PZC of adsorbent to a low value of adsorbent after adsorption of arsenic implied the formation of inner-sphere complexes between arsenic and adsorbent.

## Acknowledgments

This work was jointly supported by National Basic Research Program of China (2009CB421605); National High Technology Research and Development Program of China (2007AA06A407); the National Natural Science Foundation of China (20877079, 20921063).

## References

[1] D. Mohan, C.U. Pittman Jr., Arsenic removal from water/wastewater using adsorbents – a critical review, J. Hazard. Mater. 142 (2007) 1–53.
[2] M.E. Pena, X.G. Meng, G.P. Korfiatis, C.Y. Jing, Adsorption mechanism of arsenic on nanocrystalline titanium dioxide, Environ. Sci. Technol. 40 (2006) 1257–1262.
[3] Y. Masue, R.H. Loeppert, T.A. Kramer, Arsenate and arsenite adsorption and desorption behavior on coprecipitated aluminum:iron hydroxides, Environ. Sci. Technol. 41 (2007) 837–842.
[4] G.S. Zhang, J.H. Qu, H.J. Liu, R.P. Liu, R.C. Wu, Preparation and evaluation of a novel Fe–Mn binary oxide adsorbent for effective arsenite removal, Water Res. 41 (2007) 1921–1928.
[5] N. Balasubramanian, T. Kojima, C. Srinivasakannan, Arsenic removal through electrocoagulation: kinetic and statistical modeling, Chem. Eng. J. 155 (2009) 76–82.
[6] J. Kim, M.M. Benjamin, Modeling a novel ion exchange process for arsenic and nitrate removal, Water Res. 38 (2004) 2053–2062.
[7] J.M. Triszcz, A. Porta, F.S.G. Einschlag, Effect of operation conditions on iron corrosion rates in zero-valent iron systems for arsenic removal, Chem. Eng. J. 150 (2009) 431–439.
[8] Y.H. Weng, H.C. Lin, H.H. Lee, K.C. Li, C.P. Huang, Removal of arsenic and humic substances (HSs) by electro-ultrafiltration (EUF), J. Hazard. Mater. 122 (2005) 171–176.
[9] S.M. Maliyekkal, L. Philip, T. Pradeep, As (III) removal from drinking water using manganese oxide-coated-alumina: performance evaluation and mechanistic details of surface binding, Chem. Eng. J. 153 (2009) 101–107.
[10] M.N. Amin, S. Kaneco, T. Kitagawa, A. Begum, H. Datsumata, T. Suzuki, K. Ohta, Removal of arsenic in aqueous solutions by adsorption onto waste rice husk, Ind. Eng. Chem. Res. 45 (2006) 8105–8110.
[11] M.P.E. González, J. Mattusch, W.D. Einicke, R. Wennrich, Sorption on natural solids for arsenic removal, Chem. Eng. J. 81 (2001) 187–195.
[12] Y. Zhang, M. Yang, X.M. Dou, Arsenate adsorption on an Fe–Ce bimental oxide adsorbent: role of surface properties, Environ. Sci. Technol. 39 (2005) 7246–7253.
[13] E. Deschamps, V.S.T. Ciminelli, W.H. Höll, Removal of As (III) and As (V) from water using a natural Fe and Mn enriched sample, Water Res. 39 (2005) 5212–5220.
[14] G.S. Zhang, J.H. Qu, H.J. Liu, R.P. Liu, G.T. Li, Removal mechanism of As by a novel Fe–Mn binary oxide adsorbent: oxidation and sorption, Environ. Sci. Technol. 41 (2007) 4613–4619.
[15] Z.M. Gu, B.L. Deng, J. Yang, Synthesis and evaluation of iron-containing ordered mesoporous carbon (FeOMC) for arsenic adsorption, Microporous Mesoporous Mater. 102 (2007) 265–273.
[16] K. Gupta, U.C. Ghosh, Arsenic removal using hydrous nanostructure iron (III)–titanium (IV) binary mixed oxide from aqueous solution, J. Hazard. Mater. 161 (2009) 884–892.
[17] H. Zeng, B. Fisher, D.E. Giammar, Individual and competitive adsorption of arsenate and phosphate to a high-surface-area iron oxide-based sorbent, Environ. Sci. Technol. 42 (2008) 147–152.
[18] C.T. Yavuz, J.T. Mayo, W.W. Yu, A. Prakash, J.C. Falkner, S. Yean, L. Cong, H.J. Shipley, A. Kan, M. Tomson, D. Natelson, V.L. Colvin, Low-field magnetic separation of monodisperse $Fe_3O_4$ nanocrystals, Science 314 (2006) 964–967.
[19] J.T. Mayo, C. Yavuz, S. Yean, L. Cong, H. Shipley, W. Yu, J. Falkner, A. Kan, M. Tomson, V.L. Colvin, The effect of nanocrystalline magnetite size on arsenic removal, Sci. Technol. Adv. Mater. 8 (2007) 71–75.
[20] Z.Y. Ma, Y.P. Guan, H.Z. Liu, Synthesis and characterization of micron-sized monodisperse superparamagnetic polymer particles with amino groups, J. Polym. Sci. Polym. Chem. 43 (2005) 3433–3439.
[21] S. Dixit, J.G. Hering, Comparison of Arsenic (III) and Arsenic (V) sorption onto iron oxide minerals: implications for arsenic mobility, Environ. Sci. Technol. 37 (2003) 4182–4189.
[22] S. Sarkar, L.M. Blaney, A. Gupta, D. Ghosh, A.K. Sengupta, Arsenic removal from groundwater and its safe containment in a rural environment: validation of a sustainable approach, Environ. Sci. Technol. 42 (2008) 4168–4273.
[23] H.W. Nesbitt, G.W. Canning, G.M. Bancroft, XPS study of reductive dissolution of 7Å-birnessite by $H_3AsO_3$, with constraints on reaction mechanism, Geochim. Cosmochim. Acta 62 (1998) 2097–2110.
[24] Y. Kim, C. Kim, N. Choi, S. Rengaraj, J. Yi, Arsenic removal using mesoporous alumina prepared via a templating method, Environ. Sci. Technol. 38 (2004) 924–931.
[25] C. Su, R.W. Puls, Arsenate and arsenite removal by zerovalent iron: effect of phosphate, silicate, carbonate, borate, sulfate, chromate, molybdate, and nitrate, relative to chloride, Environ. Sci. Technol. 35 (2001) 4562–4568.
[26] P. Lakshmipathiraj, B.R.V. Narasimhan, S. Prabhakar, G.B. Raju, Adsorption of arsenate on synthetic goethite from aqueous solutions, J. Hazard. Mater. 136 (2006) 281–287.